# Photoreductive Electron Transfers in Nanoarchitectonics Organization Between a Diketopyrrolopyroleplatinum(II)-Containing Organometallic Polymer and Various Electron Acceptors

Gabriel Marineau-Plante, Malak Qassab, Adrien Schlachter, Mélodie Nos, Muriel Durandetti, Julie Hardouin, Cyprien Lemouchi, Loïc Le Pluart, Pierre Harvey

▶ **To cite this version:**

Gabriel Marineau-Plante, Malak Qassab, Adrien Schlachter, Mélodie Nos, Muriel Durandetti, et al.. Photoreductive Electron Transfers in Nanoarchitectonics Organization Between a Diketopyrrolopyroleplatinum(II)-Containing Organometallic Polymer and Various Electron Acceptors. Journal of Inorganic and Organometallic Polymers and Materials, 2022, 32, pp.1266. 10.1007/s10904-021-02170-3 . hal-03619511

**HAL Id: hal-03619511**

**https://normandie-univ.hal.science/hal-03619511v1**

Submitted on 12 Sep 2024

**HAL** is a multi-disciplinary open access archive for the deposit and dissemination of scientific research documents, whether they are published or not. The documents may come from teaching and research institutions in France or abroad, or from public or private research centers.

L'archive ouverte pluridisciplinaire **HAL**, est destinée au dépôt et à la diffusion de documents scientifiques de niveau recherche, publiés ou non, émanant des établissements d'enseignement et de recherche français ou étrangers, des laboratoires publics ou privés.

# Photoreductive Electron Transfers Between a Diketopyrrolopyroleplatinum(II)-Containing Organometallic Polymer and Various Electron Acceptors

Gabriel Marineau-Plante,[a] Malak Qassab[b], Adrien Schlachter,[a] Mélodie Nos,[b] Muriel Durandetti,[c] Julie Hardouin,[d,e] Cyprien Lemouchi,*[b] Loïc Le Pluart,*[b] Pierre D. Harvey,*[a]

[a]*Département de chimie, Université de Sherbrooke, Sherbrooke, PQ, Canada J1K 2R1. E-mail: Pierre.Harvey@USherbrooke.ca*

[b]*LCMT UMR CNRS 6507, Normandie Université, UNICAEN, ENSICAEN, CNRS, 14000 Caen, France. E-mail: cyprien.lemouchi@ensicaen.fr, loic.le_pluart@ensicaen.fr*

[c]*COBRA UMR CNRS 6014, Normandie Université, UNIROUEN, INSA Rouen, CNRS, 76000 Rouen, France. Email : muriel.durandetti@univ-rouen.fr*

[d]*PBS UMR CNRS 6270, Normandie Université, UNIROUEN, 76821 Mont Saint Aignan, France. Email : julie.hardouin@univ-rouen.fr*

[e]*PISSARO Proteomic Facility, IRIB, F-76820 Mont-Saint-Aignan, France*

## Introduction

Diketopyrrolopyrrole (DPP)-based conjugated polymers represent an important class of donor materials in the design of performant organic solar cells (OSCs),[1-3] and the high electrical mobility they can display makes them attractive for thin-film transistor technology, as well.[4] Over the past several years, platinum(II) polyyne versions of DPP-containing polymers were investigated (see general structure in **Figure 1**),[5,6] but their photoconversion efficiencies (PCE) were found to be modest not exceeding 1.4% (**P1-P5**), using 3'H-cyclopropa[1,9][5,6]-fullerene-C60-Ih-3′-butanoic acid 3′-phenyl methyl ester ($PC_{61}BM$) as electron acceptor. These results contrast with those recently obtained with **P6** (PCE = 7.36%)[7] and **P7** (PCE = 9.54%)[7] and other **Pn** (with R = Bu, $R^1$ = mesogenic-containing group, $R^2$ = H, m = 0; 8.13 ≤ PCE ≤ 9.62%) using [6,6]-phenyl-$C_{71}$-butyric acid methyl ester, $PC_{71}BM$, as electron acceptor.[8] In fact, the PCE increases upon modulating the structure of the donor platinum(II) polyyne polymers and the nature of the electron acceptor, which affect the relative energy positioning of the frontier MOs.

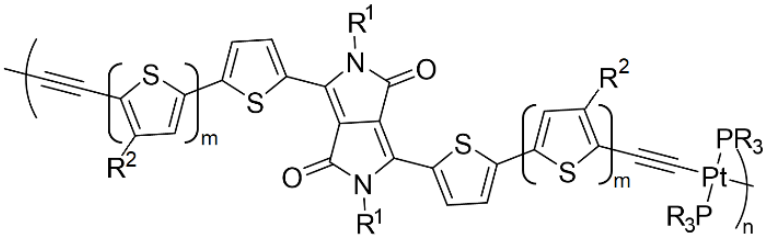

**P1** (R = Et, $R^1$ = n-$C_8H_{17}$, $R^2$ = $C_6H_{13}$, m = 0)[5]
**P2** (R = Et, $R^1$ = 2-ethylhexyl, $R^2$ = $C_6H_{13}$, m = 0)[5]
**P3** (R = Et, $R^1$ = 2-ethylhexyl, $R^2$ = $C_6H_{13}$, m = 1)[5]
**P4** (R = Bu, $R^1$ = 2-ethylhexyl, $R^2$ = H, m = 0)[6]
**P5** (R = Bu, $R^1$ = 2-ethylhexyl, $R^2$ = H, m = 1)[6]
**P6** (R = Bu, $R^1$ = n-$C_9H_{19}$, $R^2$ = H, m = 0)[7]

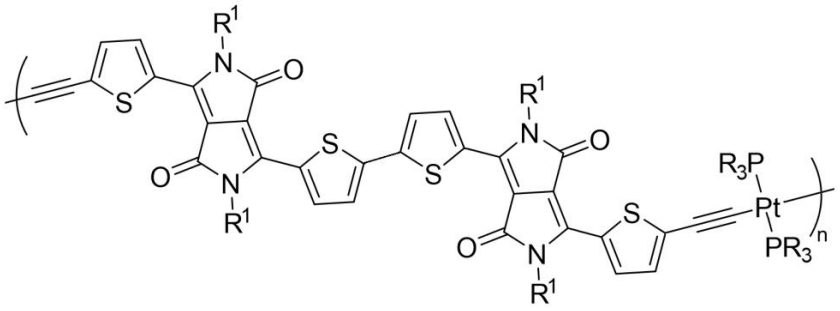

**P7** (R = Bu, $R^1$ = n-$C_9H_{19}$)[7]

**Figure 1**. Selected structures of diketopyrrolopyrrole-platinum(II) polyyne-based conjugated polymers investigated in the literature.

The generally accepted initial photo-oxidative process in the donor-acceptor active layer consists in an electron transfer from the polymer donor to the acceptor ($^1$polymer* + acceptor → polymer$^{+\bullet}$ + acceptor$^{-\bullet}$) where the polymer is a platinum(II) polyyne and acceptor is a fullerene such as $PC_{61}BM$). These photo-induced processes are known to occur in the femtosecond time scale, and the back electron transfer (polymer$^{+\bullet}$ + acceptor$^{-\bullet}$ → $^3$polymer* + polymer + acceptor) occurs in the picosecond range.[7-9] A large part of these short time scales is due to the rather efficient exciton migration across the conjugated platinum(II) polyyne chain.[10]

It was recently argued on a thermodynamic ground that besides the photo-oxidative process, a parallel photo-reducing process (polymer + $^1$acceptor* → polymer$^{+\bullet}$ + acceptor$^{-\bullet}$) could also take place since both the donor polymer and acceptor molecule are subjected to irradiation at the same time.[11,12] By ignoring the fill factor (FF) parameter associated with the morphology of the blend, if the acceptor molecule is a nonfullerene (generally constructed on a push-pull ADA design where A and D are electron withdrawing and donating groups, respectively), then its intrinsic larger absorptivity's in the visible region allow for a accentuated photon harvesting by the OSC. This phenomenon results in an increase in PCE with respect to those obtained when the photonic device built with fullerenes ($PC_{61}BM$ and $PC_{71}BM$), which do not exhibit large absorptivity values in the visible.

We now report an explanation as why small PCEs are obtained in some OSCs, notably for **P1-P5**, based on thermodynamic data. The selected example consists in a diketopyrrolopyrrole-platinum(II) polyyne reminiscent of those illustrated in **Figure 1** where R = Bu, $R^1$ = n-$C_9H_{19}$, $R^2$ = H, m = 0 (**P**) as polymer donor, and two common fullerenes ($PC_{61}BM$ and $PC_{71}BM$) as well as one nonfullerene molecule (**MCzM**;[13] **Figure 2**) as acceptor.

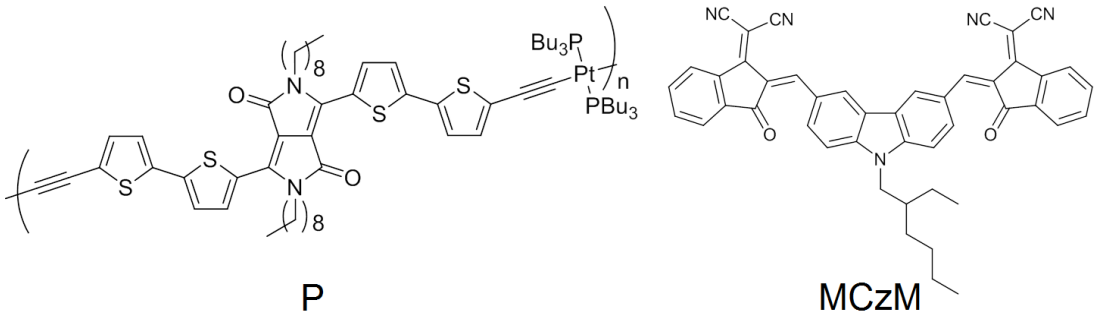


**Figure 2**. Structures of the polymer donor **P** and nonfullerene acceptor **MCzM**.

## Experimental section

This section is placed in the Supporting Information. It contains full characterizations of the intermediates and new products.

## Results and Discussion

**Ligand synthesis L** was synthesized in five steps from 2-thiophencarbonnitrile using a modified procedure applied for similar compound preparation[14]. The difference into their molecular structure is the side chain on the DPP group. For **L** linear chain *n*-$C_9H_{19}$ was privileged to 2-ethylhexyl branched chain[14] in order to improve chains aggregation and should be more favourable for electronic properties enhancements. **L** was synthesized according to scheme 1. The synthesis of the dibrominated DPP **1** was already reported in our previous work[15]. Four thiophenes containing DPP (DPP-T4) **2** was prepared from compound **1** by Pd-catalyzed Stille coupling reaction in 60 % yield. The second step, a bromination with NBS, is the limiting step. Even when applying literature procedures[14-16], the compound was isolated with lower yields and the reaction suffers from lack of reproducibility, it might be due to a low reactivity and instability issues of brominated compounds **3** and **3'**. But, better yields were obtained when using bromine instead of NBS. The changes made to a reported procedure[17] significantly improve the yields, by keeping the reaction temperature below 0°C and reducing the reaction time. A mixture of mono- and dibrominated compounds **3'** and **3** was obtained as detected by MALDI-TOF/MS, it was directly engaged in the final step because of high difficulties encountered to separate them. Lastly, Sonogashira coupling reaction between trimethylsilylacetylene (TMSA) and brominated compounds **3** and **3'** leads to dark blue solid as the ligand **L** in 41 % average yield after two steps from **2**. It was characterized by $^{1}H$ and $^{13}C$ NMR (Fig. S1 and S2, ESI), high-resolution electrospray ionization mass spectrometry (HRMS) (Fig. S3, ESI) and attenuated total reflection infrared (ATR IR) (Fig. S5, ESI) and

**P** was synthesized from ligand **L** (Scheme 1). **P** was prepared using a CuI-catalyzed dehydrohalogenation reaction between ligand **L** and freshly prepared *trans*-dichlorobis(tri-n-butyphosphine)platinium (II), *trans*-[$PtCl_2(PBu_3)_2$]. Metallooligomer formation was confirmed by $^{1}H$ NMR. After complexation of ligand **L** to Pt(II)-complex, expected upfield chemical shift of thiophen-terminated proton H4 nearby the triple bond of -0.38 ppm was

observed, in contrast to more remote H3 nearby DPP core, which is not affected (Fig. S8, ESI). $^{31}P\{^{1}H\}$ NMR spectrum displays an intense signal at 3.55 ppm with a coupling constant J($^{31}P$-$^{195}Pt$) of 2306 Hz, which is consistent with trans-geometry of the metallooligomers **P**, similar to **P3** (3.58 ppm, 2332 Hz)[6], (Fig. S9 ESI). Comparison of IR-ATR spectra of ligand **L** and polymer **P** brings out vibration frequency decrease of the band ν(C≡C) from 2140 to 2083 $cm^{-1}$ attributed to back-bonding effect (Fig. S5 and S10, ESI). According to reported procedure[15], reaction between *trans*-[$PtCl_2(PBu_3)_2$] (1 eq.) and CuI (1eq.) for three days yields to short chain metallooligomers with an average molecular mass ($M_n$) of 12.4 $kg.mol^{-1}$ corresponding to 9-10 units with a dispersity Đ of 2.3, which is higher what is obtained for **P5** ($M_n$=8.8 $kg.mol^{-1}$, Đ = 2.3) but lower than for **P6** ($M_n$=18.2 $kg.mol^{-1}$, Đ = 2.1) and **P3** ($M_n$=22.1 $kg.mol^{-1}$, Đ = 2.2). Longer polymer chains **P'** with $M_n$ of 23.8 $kg.mol^{-1}$ (17-18 units) and a dispersity of 2.8 were prepared from a modified procedure using higher molar quantity of CuI from (0.5 eq instead of 0.1 eq.). and larger excess of ligand **L** (1.79 eq. instead of 1 eq.) (Fig. S11, ESI). The polymers were characterized by MALDI-TOF/MS with the 2-[(2E)-3-(4-*tert*-butylphenyl)-2-methylprop-2-enylidene]malononitrile (DCTB) matrix. The spectrum displays ion series from m/z 1000 to 9000 with mass gap of 1360-1362 Da, which is equal to molecular mass of the repeating unit. The analysis confirmed the formation of oligomers comprised of six units at least (Fig. S12, ESI). $^{31}P\{^{1}H\}$ NMR spectrum of **P** consists of a second low intense signal at 7.5 ppm attributed to end-chain **L**-$Pt(PBu_3)_2$-Cl, which is not present in spectrum of **P'**(Fig. S9, ESI). It is in good agreement with shorter length of chains for **P** and longer ones for **P'**. Thermogravimetric analyses (TGA) of **P** and **P'** indicates a decomposition temperature of 273 °C, a higher thermal stability than **P6** ($T_d$ = 221°C) but similar to **P3** ($T_d$ =283 °C) (Fig. S13, ESI).

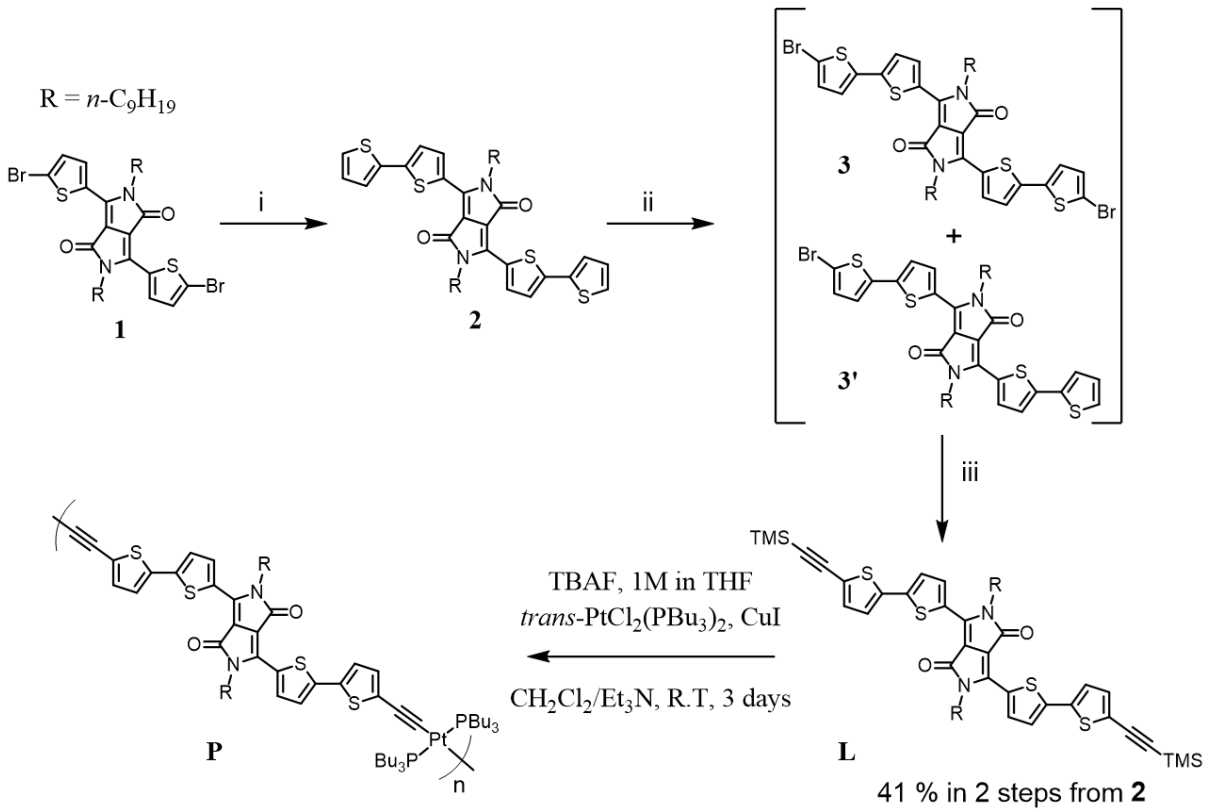


**Scheme 1**: Synthetic Scheme for **P**. (i) 2-(tributylstannyl)thiophen (2.5 eq.) , $Pd(PPh_3)_2Cl_2$ (10 mol%), $PPh_3$ (20 mol%), toluene, reflux, overnight, *60 % yield*. (ii) $Br_2$ (2 eq.), T < 0°C, $CHCl_3$, 3 hrs. (iii) TMSA, $Pd(PPh_3)_2Cl_2$, CuI, THF/$(iPr)_2NH$, 70°C, 3hrs.

*Electrochemistry and HOMO and LUMO energies*. **P** and **MCzM** are new compounds and were characterized by electrochemistry along with **MCzM**, in order to localize the HOMO and LUMO. The cyclic voltamograms (CVs) of **P** and **MCzM** are placed in the ESI, Figures S15 and S16 but the necessary data are placed in Table 1. The CV of **P** exhibits chemically reversible waves in both the oxidation and reduction sides. The oxidation peak is placed at +1.07 V (anodic sweep) and a reduction peak signal is detected at -1.20 V (cathodic sweep) *vs* SCE (**Figure 4**). The onset potentials are respectively evaluated at +0.71 and -1.00 V *vs* SCE, thus placing the HOMO and LUMO at -5.44 and -3.73 eV, respectively. This bandgap ($E_g^{elec.}$ = 1.71 eV) matches well the valuet evaluated from the onset of the lowest energy band of the absorption spectrum (Figure 5; $E_g^{opt}$ = 1.60 eV). The obtained values are compared with values from the literature for both **MCzM** and **P** (see **P3** for a close analogue). The data of **Table 1** exhibit close similarities with the literature data, but also several discrepancies, notably for $E_{LUMO}$.

**Table 1**. Electrochemical data, HOMO and LUMO energies, and band gaps of, **MCzM** and **P**, and comparison with literature data.

| | **MCzM** | **MCzM** (ref.13) | **P** | **P3 (**ref.5) |
|---|---|---|---|---|
| $E_{ox}$ (V) [a] | +1.89 | +0.93 (*vs* $Fc/Fc^+$) | +1.07 | not reported |
| $E_{ox}^{onset}$ (V) [a] | +1.30 | not reported | +0.71 | +0.77 (*vs* Ag/AgCl)[d] |
| $E_{HOMO}$ (eV)[b] | -6.03 | -6.08 | -5.44 | -5.49 |
| $E_{red}^{a}$ (V) [a] | -0.93 | -1.25 (*vs* $Fc/Fc^+$) | -1.20 | not reported |
| $E_{red}^{onset}$ (V) [a] | -0.67 | not reported | -1.00 | -1.18 (*vs* Ag/AgCl)[d] |
| $E_{LUMO}$ (eV) [b] | -4.06 | -3.79 | -3.73 | -3.54 |
| $E_g$ (eV)[c] | 2.82 | 2.18 | 2.27 | — |
| $E_g^{onset}$ (eV)[c] | 1.97 | — | 1.71 | 1.96 |
| $E_g^{av}$ (eV)[c] | 2.40 | — | 1.99 | — |
| $E_g^{opt}$ (eV)[c] | 2.11 | 2.10 | 1.72 | 1.69 |

[a] $E_{ox}$ = oxidation peak potential, $E_{ox}^{onset}$ = oxidation onset, $E_{red}$ = reduction peak potential, $E_{red}^{onset}$ = reduction onset, potential *vs* SCE .
[b] $E_{HOMO} = -(E_{ox} + 4.73)$, $E_{LUMO} = -(E_{red} + 4.73)$. [c] $E_g = (E_{ox} - E_{red})$, $E_g^{onset} = (E_{ox}^{onset} - E_{red}^{onset})$, $E_g^{av} = (E_g + E_g^{onset})/2$, $E_g^{opt}$ = optical $E_g$. [d] No cyclic voltamogram was provided in this work.

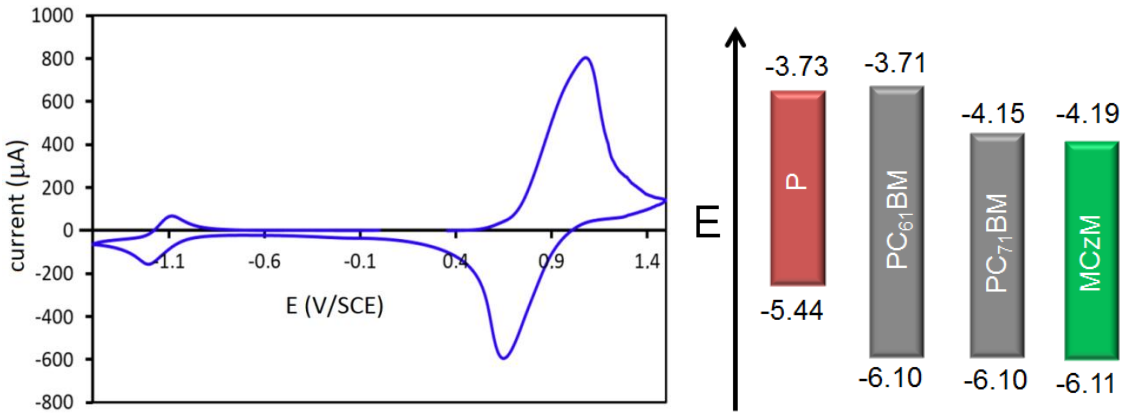


**Figure 4**. Left: CVs of the **P** metallooligomers. The oligomers thin films were cast from a $CH_2Cl_2$ solution onto a platinum disc working electrode (d = 5 mm), and the CVs were recorded in $CH_3CN$ solution containing $NBu_4PF_6$, $10^{-1}$ mol.$L^{-1}$ as supporting electrolyte (scan rate of 50 mV.$s^{-1}$). Right: Energy diagram reporting the HOMO and LUMO energies based on $E_{ox}^{onset}$ and $E_{red}^{onset}$ values of **P** and **MCzM**, and those of $PC_{61}BM$ and $PC_{71}BM$. Note that the most recently reported HOMO and LUMO energies of the two latter fullerenes vary a little. For example, the ELUMO for $PC_{61}BM$ and $PC_{71}BM$ vary from -3.70 to -3.75 and from -4.10 to -4.20 eV, respectively. In these cases, average values are used.

The CVs of **MCzM** exhibit ill-defined irreversible waves indicating reactivity (Figure placed in the SI). The onsets permit an approximate evaluation of its HOMO and LUMO energies (Table 1). Its $E_g^{onset}$ value is 1.97 eV, which is quite low compared to the $E_g^{opt}$ by ~0.1 eV, *i.e.* 2.11 eV. This is very likely due to the ill-defined shapes of the oxidation and reduction waves. By calculating bandgaps based on the peak maxima (called peak potentials), a larger $E_g$ value of 2.33 eV is calculated (*i.e.* overshoot). It appears that averaging $E_g$ and $E_g^{onset}$ ($E_g^{av}$) leads in this case to a better comparison with $E_g$ (~2.13 eV). Using the $E_{ox}^{onset}$ and $E_{red}^{onset}$ values of **P** and **MCzM**, an energy diagram comparing the $E_{HOMO}$ and $E_{LUMO}$ is built (**Figure 4**,right), and compared to those of $PC_{61}BM$[18-22] and $PC_{71}BM$.[23-27] The conclusions are three folds. First the energies of the frontier MOs of the nonfullerene are similar to those of $PC_{71}BM$. Second, $E_{LUMO}$ for **P** and $PC_{61}BM$ are similar, meaning that oxidative photo-induced electron transfer ($^1P^* + PC_{61}BM \rightarrow {}^1P^{+\bullet} + PC_{61}BM^{-\bullet}$) would be slow and excited state quenching of $^1$**P*** would be partial, if any. Third, the reductive photo-induced electron transfer ($^1P^*$ + acceptor $\rightarrow$ $^1P^{+\bullet}$ + acceptor$^{-\bullet}$) is thermodynamically favorable.

*UV-vis spectra of **P2***. The absorption spectra of **P** in solution and as thin films have been interpreted though their comparison with the absorption spectrum of **L**, and through DFT and TDDFT computations (**Figure 5**). The low-energy band of **L** (black line) exhibits a maximum at ~634 nm. This band shifts to ~665 nm (blue line) in **P**, which is consistent with the extension of the π-system through the C≡CP($PR_3$)$_2$C≡C unit. As a film, this band shifts to ~690 nm (red line), which is consistent with aggregation with π–π contacts.

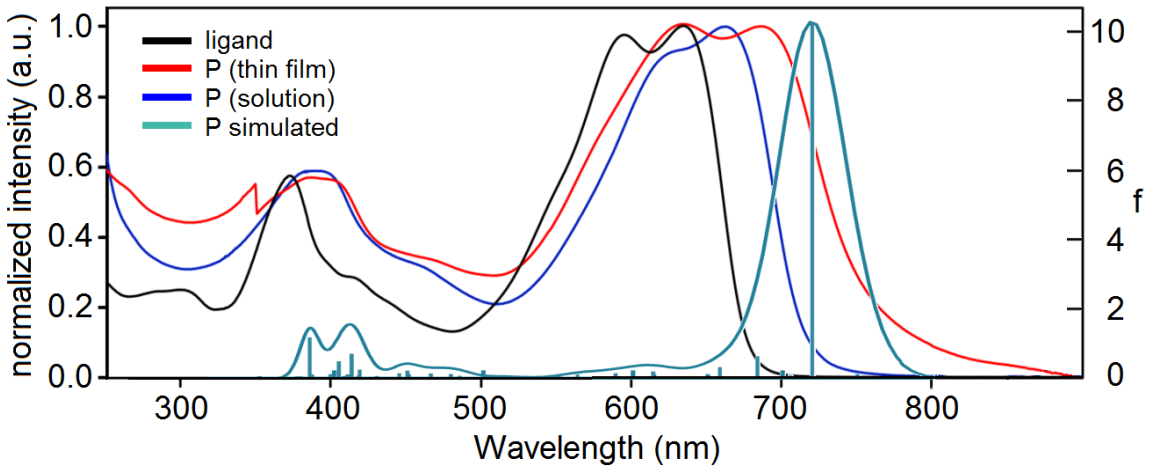


**Figure 5**. Normalized absorption spectra of **L**, **P** in $CH_2Cl_2$ , **P** as a thin film on a glass plate (spin coating), and bar graph reporting the oscillator strength (f) and position of the electronic transitions calculated by TDDFT for **P** (in turquoise). The turquoise line is a simulated spectrum with an arbitrary thickness of 1500 $cm^{-1}$ for each transition (*i.e.* each bar). Note that no vibronic component is included in this calculated spectrum.

The geometry of H-**L**-[Pt($PBu_3$)$_2$-**L**]$_4$-H where **L** = C≡C-thiophene-DPP-thiophene-C≡C, used as model for **P** was optimized using DFT computations. This model is selected since it is the largest possible molecule that could be handled by the supercomputer while keeping a good accuracy of the 6-31g* basis sets. Spiral-type 1D-chain resulted from the geometry optimization (see SI). Selected frontier MO representations are provided in **Figure 6** and the relative atomic contributions separated by fragment are summarized in **Table 2**. The atomic contributions of the frontier MOs are largely localized on the DPP and thiophene units and are fully consistent with the presence of an extended π-system. The extension of the π-system is well apparent in the HOMO where the atomic contributions spread over the three central units including the four platinum atoms.

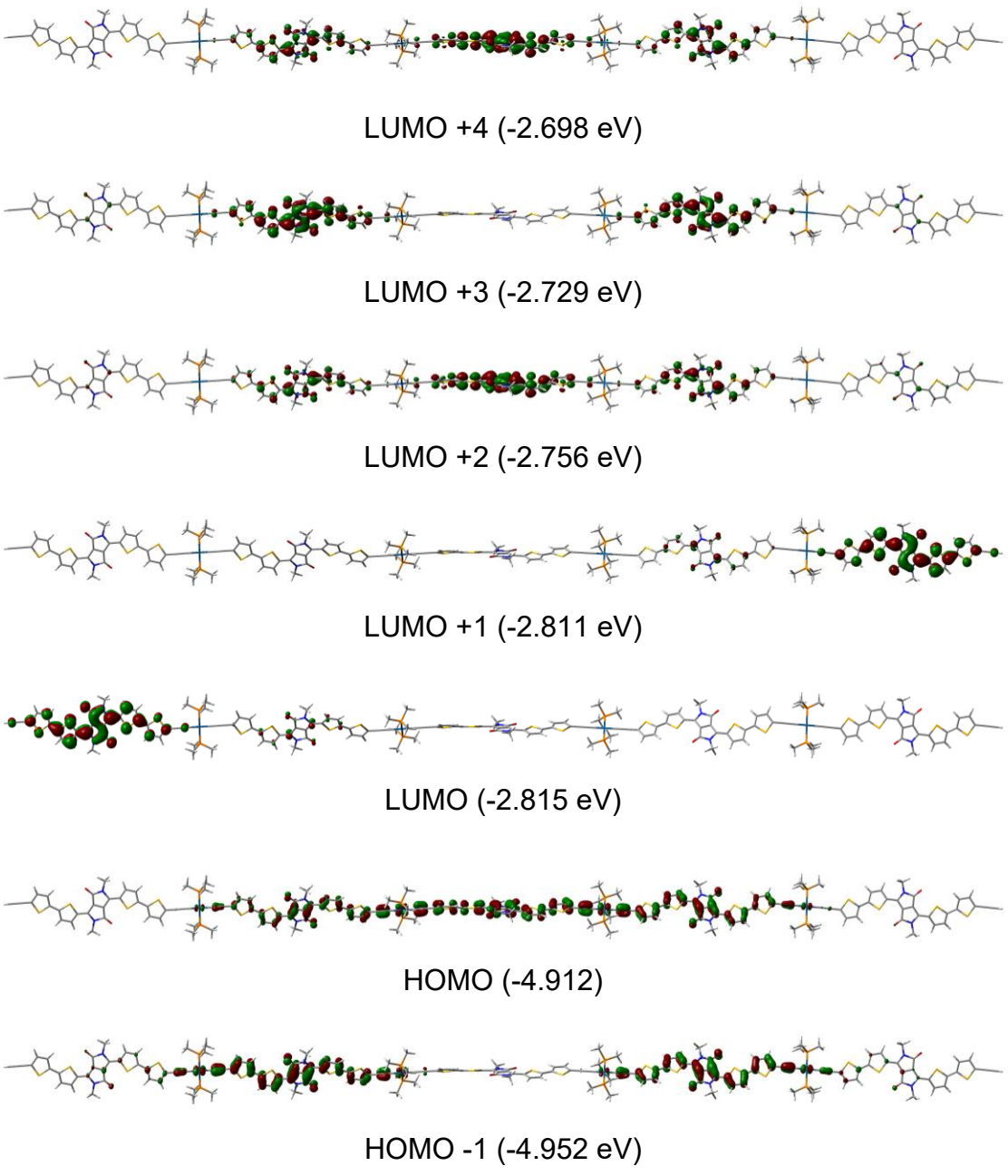


**Figure 6**. Representations of the frontier MOs of **P** (HOMO+2 to +4 are placed in the SI).

**Table 2**: Relative atomic contributions (%) of the fragments to the frontier MOs of **P**.[a)]

| Fragments | H-4 | H-3 | H-2 | H-1 | HOMO | LUMO | L+1 | L+2 | L+3 | L+4 |
|---|---|---|---|---|---|---|---|---|---|---|
| DPP | **46.6** | 41.0 | 36.4 | 32.8 | 31.2 | 43.4 | 43.6 | 43.8 | 44.6 | 45.5 |
| thiophene | 46.3 | **46.7** | **48.7** | **49.6** | **50.1** | **50.7** | **53.1** | **52.4** | **51.8** | **51.2** |
| $PBu_3$ | 0.2 | 0 .2 | 0.4 | 0.3 | 0.4 | 0.3 | 0.3 | 0.5 | 0.3 | 0.2 |
| Pt | 1.1 | 3.2 | 4.6 | 6.0 | 6.5 | 0.4 | 0.4 | 0.7 | 0.8 | 0.9 |
| C≡C | 5.8 | 8.9 | 9.9 | 11.3 | 11.9 | 5.2 | 2.7 | 2.6 | 2.5 | 2.2 |

a) The values in bold are the largest ones (H = HOMO; L = LUMO).

The filled MOs exhibit larger atomic contributions on the (C≡C)Pt($PBu_3$)$_2$(C≡C) unit than that of the empty one, so that low-energy electronic transitions are largely of a ππ* type, mixed with some metal-to-ligand charge transfer, MLCT, where M is (C≡C)Pt($PBu_3$)$_2$(C≡C), **[Pt]**, and L is DPP and thiophene. This outcome is consistent with the fact that **[Pt]** is electron rich and DPP is an electron attracting group, which is consistent with the push-pull design. Concurrently, TDDFT computations place the lowest energy transition at 720 nm (**Table 3**), which matches the onset value of 785 nm corresponding to $E_g^{opt}$ = 1.58 eV(Table 1). In conclusion, the lowest energy singlet excited state is a ππ* state (major) mixed with MLCT (minor).

**Table 3**: Calculated position, oscillator strength (f) and major contributions of the first five spin-allowed electronic transitions of H-**L**-[Pt($PBu_3$)$_2$-**L**]$_4$-H (optimized geometry).[a)]

| λ (nm) | f | Major contributions (%) (H = HOMO; L = LUMO) |
|---|---|---|
| 719.9 | 10.23 | H-1→L+3 (17), HOMO→L+2 (40) |
| 705.1 | 0.081 | H-1→LUMO (13), H-1→L+2 (12), HOMO→L+3 (20) |
| 683.1 | 0.629 | HOMO→L+2 (15), HOMO→L+4 (16) |
| 664.7 | 0.011 | H-4→L+1 (10), H-3→LUMO (15), H-1→L+2 (15), HOMO→L+3 (18) |
| 658.1 | 0.314 | H-2→L+2 (15), H-1→L+3 (23), HOMO→L+4 (27) |

a) See SI for the first 100 spin-allowed transitions.

*DFT computations of the oxidized and reduced forms of **P***. The nature of the oxidized and reduced forms of **P** were addressed by DFT using the models [H-**L**-[Pt($PBu_3$)$_2$-**L**]$_4$-H]$^+$ • and [H-**L**-[Pt($PBu_3$)$_2$-**L**]$_4$-H]$^-$ • (**Figure 7**). The SOMO of the anion exhibits atomic contributions localized on one **L** end-group with no atomic contributions from the Pt($PBu_3$)$_2$ fragment, which is reminiscent of what is observed for the LUMO and LUMO+1 of **P** (**Figure 6**). Conversely, the SOMO of the cation exhibits atomic contributions localized on one central [Pt($PBu_3$)$_2$-**L**] unit only thus indicating of a lesser extensive π-system than that of the HOMO of [H-**L**-[Pt($PBu_3$)$_2$-**L**]$_4$-H] (**Figure 6**). The energy difference between the two SOMOs is 1.78 eV, which is close to the $E_g^{onset}$ value evaluated

with the onset values of the oxidation and reduction waves depicted in the cyclic voltammograms of **P** ($Eg^{onset}$ = 1.71 eV; **Table 1**). In conclusion, the nature of the SOMOs of the oxidized and reduced forms of **P** are consistent with the frontier MOs deduced for the neutral H-**L**-[Pt($PBu_3$)$_2$-**L**]$_4$-H and thus shines light of the nature of the species formed during the photooxidative and -reductive processes of **P** in polymer donor / electron acceptor blends.

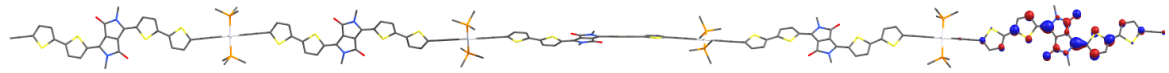

SOMO anion (-3.240 eV)

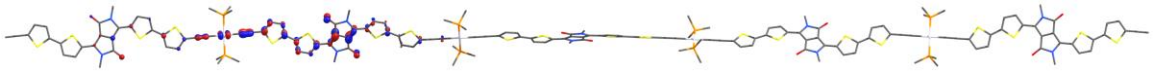

SOMO cation (-5.020 eV)

**Figure 7**. Representations of the SOMOs of [H-**L**-[Pt($PBu_3$)$_2$-**L**]$_4$-H]$^{+\bullet}$ (top) and [H-**L**-[Pt($PBu_3$)$_2$-**L**]$_4$-H]$^{-\bullet}$ (bottom).

*Photophysical properties of **P** and **MCzM***. The absorption, excitation and fluorescence spectra of **P** and **MCzM** and their properties are respectively reported in **Figure 8** and **Table 4**. Both **P** and **MCzM** as thin films are weakly fluorescent (the fluorescence quantum yields, $\Phi_F$, are respectively <0.0001 and 0.011; using an integration sphere). The assignment of the fluorescence is based on the small Stoke shifts ($\Delta\nu$) and ps-ns time scale of the fluorescence lifetimes ($\tau_{fluo}$) confirmed from solution data. The fluorescence decays are in the SI. The properties of **P** compares favorably to those of **P3**.

**Table 4**. Optical properties and photophysical data of **P** and **MCzM**.

| | $\lambda_{abs}$ (nm) | $\lambda_{fluo}$ (nm) | $\Delta\nu$ ($cm^{-1}$)[a] | $\tau_F$ (ns)[b] (f%)[c] | $\chi^2$ |
|---|---|---|---|---|---|
| **P** in $CH_2Cl_2$ | 337, 663 | 712 | 1040 | 0.10 (16.4)<br>0.43 (83.6) | 1.044 |
| **P** as thin film | 400, 691 | 712 | 430 | < 0.090[d] | — |
| **MCzM** in $CH_2Cl_2$ | 291, 324, 459, 542 | 603 | 1870 | 1.6 (47.3)<br>4.8 (52.7) | 1.079 |
| **MCzM** as thin film | 306, 342, 485, 592 | 603 | 310 | < 0.090[d] | — |

[a]$\Delta\nu = \nu_{abs} - \nu_{fluo}$ (in $cm^{-1}$) [b]The uncertainties are ± 10% based on multiple measurements.

[c] $f_i(\%) = (B_i\tau_i)/\Sigma(B_i\tau_i) \bullet 100\%$; $I_e(t) = B_1\exp(-t/\tau_1) + B_2\exp(-t/\tau_2) + B_3\exp(-t/\tau_3) + \ldots$ [d] The FWHM of the excitation source is 90ps. The emission decays are inside the pulse profile.

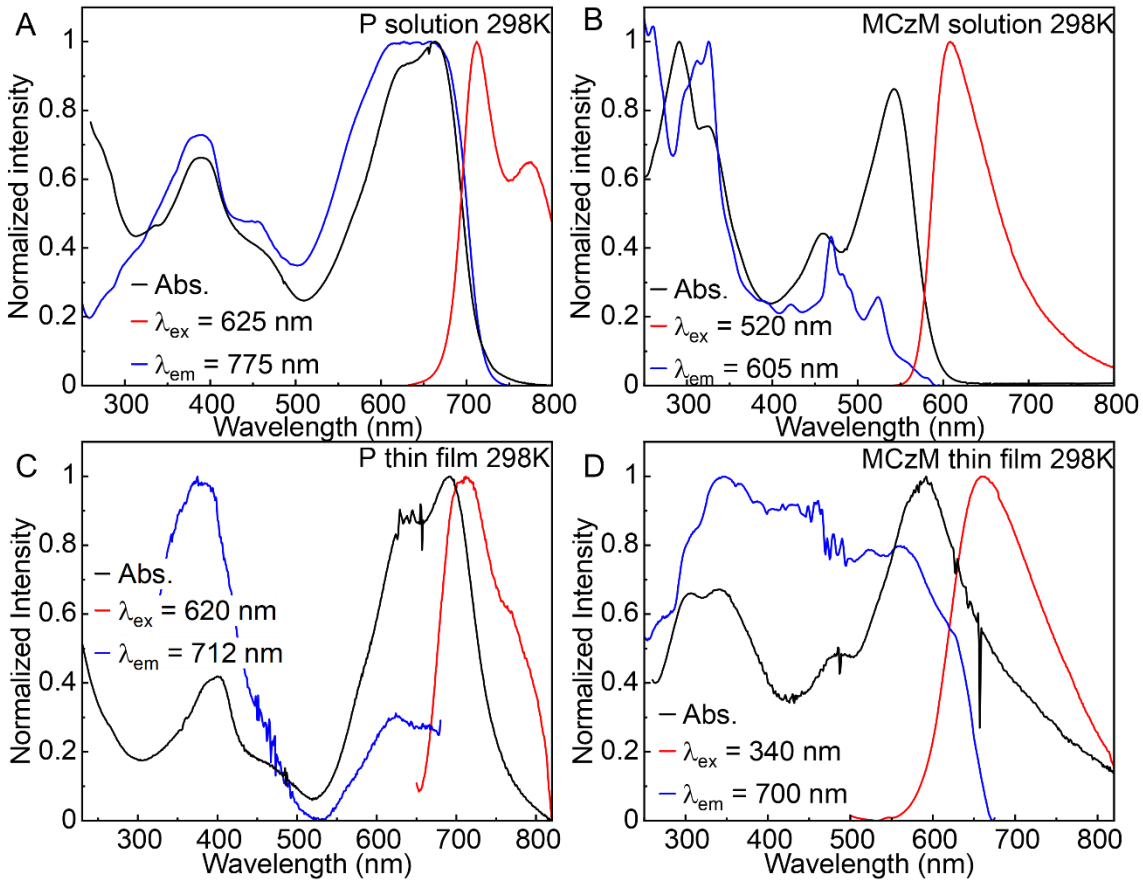


**Figure 8**. Normalized absorption (black), excitation (blue) and fluorescence (red) spectra of **P** in $CH_2Cl_2$ (A) and drop-casted thin film (C), and of **MCzM** in $CH_2Cl_2$ (B) and drop-casted thin film (D).

*Photooxidative and -reductive quenching of the blends*. Based on the thermodynamic data of **Table 1** and **Figure 4**, all photo-induced electron transfers are found to be favorable, except perhaps for the photo-oxidative process $^1\mathbf{P}^* + PC_{61}BM \rightarrow \mathbf{P}^{+\bullet} + PC_{61}BM^{-\bullet}$, which can be either inexistent or weakly favorable. Note that this slight ambiguity is due to the variabilities of (or difficulty to precisely evaluate) the HOMO and LUMO energies of $PC_{61}BM$ reported in the literature. In any case, the latter process is bound to be either nil or very slow. Moreover, fullerenes $PC_{61}BM$ and $PC_{71}BM$ suffer from low absorptivity values in the visible region. Consequently, the relative number of excitons generated by the direct excitation of the fullerene acceptors will be small, thus the proportion of photo-reductive processes will be small as well. To overcome this potential problem in this study,

the use of **MCzM** is made. Indeed, this fluorescent compound conveniently shares similar $E_{HOMO}$ and $E_{LUMO}$ values with those of $PC_{71}BM$, but exhibits a larger ε value (51000 $M^{-1}cm^{-1}$ at $\lambda_{abs}$ = 542 nm), which makes the reductive quenching operational (**P** + $^1$**MCzM*** → **P**$^{+\bullet}$ + **MCzM**$^{-\bullet}$) as well as the oxidative one. Moreover, this 542nm band is also conveniently placed in the absorption region exhibiting a minimum absorption in the **P** spectra (**Figure 8**). Upon mixing **P** with **MCzM**, both fluorescence bands that of **P** and **MCzM** are quenched (**Figure 9**) where both oxidative and reductive quenching are possible at the same time: $^1$**P*** + **MCzM** → **P**$^{+\bullet}$ + **MCzM**$^{-\bullet}$ and **P** + $^1$**MCzM*** → **P**$^{+\bullet}$ + **MCzM**$^{-\bullet}$ (note that **P**$^{+\bullet}$ + **MCzM**$^{-\bullet}$ are non-emissive). $PC_{61}BM$ and $PC_{71}BM$ are also non-emissive in the solid state based on the literature and experiments herein. Nonetheless, the same observation is made for $PC_{61}BM$- and $PC_{71}BM$-containing blends (*i.e.* efficient quenching of the **P** fluorescence band). This latter finding indicates that $PC_{61}BM$ also quenches $^1$**P***. It is also noteworthy the rate for electron transfer cannot be measured as the fluorescence lifetimes in the blends are shorter than the IRF (**Table 4**). The overall photophysical processes occurring in the blends as thin films are summarized in **Figure 10**.

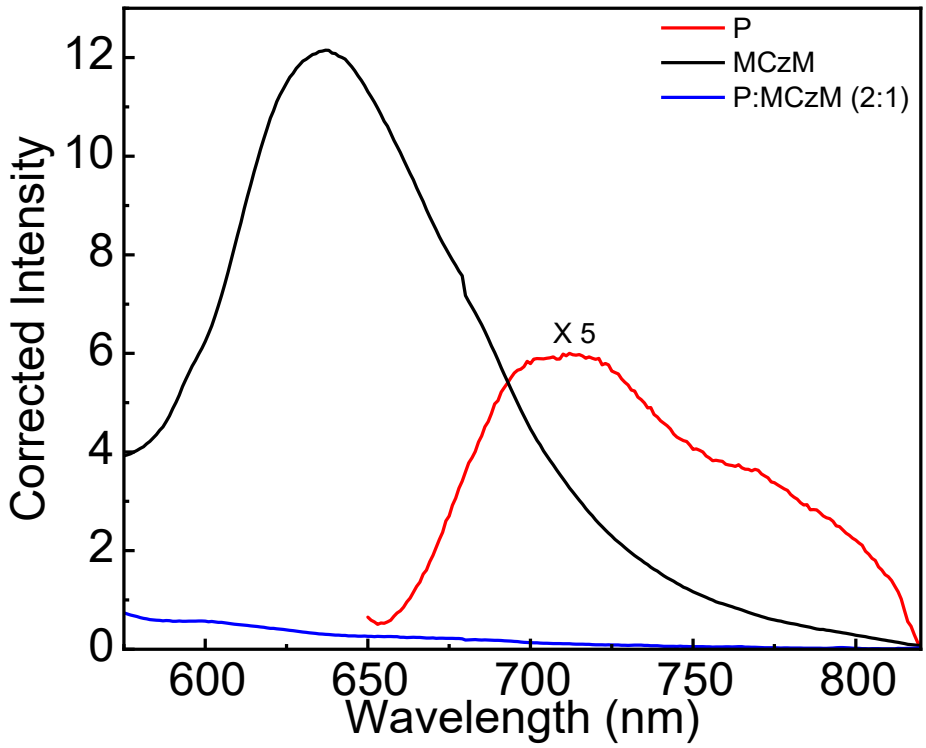

**Figure 9**: Fluorescence spectra of **P**:**MCzM** blends films (2:1). Red: Pristine **P** film. Black: Pristine **MCzM** film. Blue: 2:1 ratio of **P**:**MCzM**. $\lambda_{ex}$ for **MCzM** and **P**:**MCzM** is 477nm, and $\lambda_{ex}$ for **P** = 633nm.

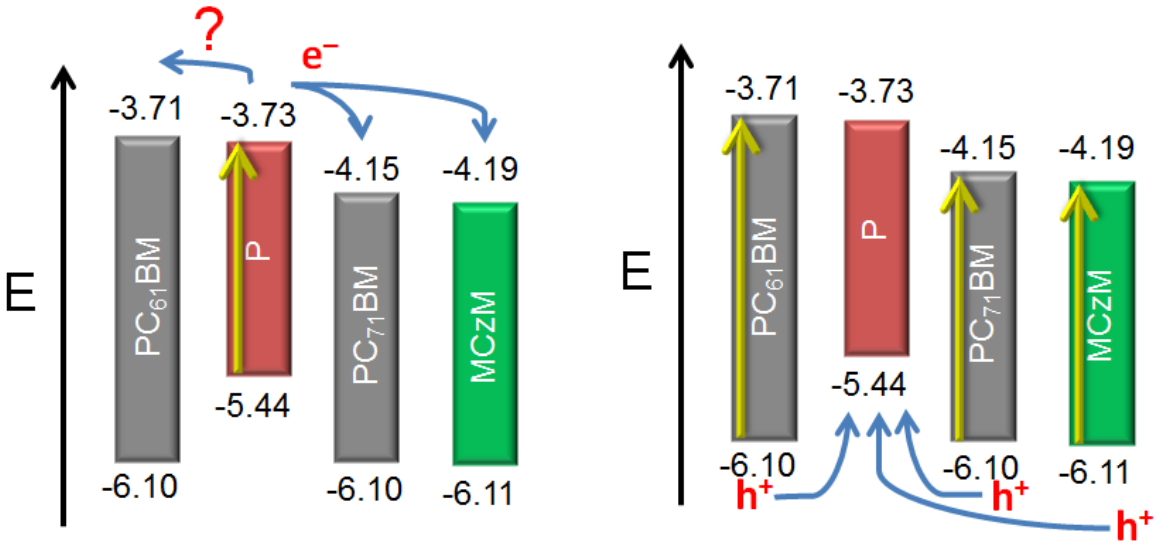


**Figure 10**. Schemes illustrating the photooxidative (left) and -reductive (right) processes. Note that the electron transfer between $^1$**P*** and **MCzM** (left hand side) is indicated as uncertain for thermodynamic reasons, but experimentally, the quenching of the emission band of **P** indicates quenching. Therefore this process occurs but is most likely slow.

These quenching experiments indicate that electron transfer does occur between $PC_{61}BM$ and $^1$**P*** to some extent. However, it does not fully explain the significant difference in PCEs between **P1-P5** (1.4%)[5,6] and **P6** (7.36%),[7] **P7** (7.36%)[7] and other **Pn** (8.13 ≤ PCE ≤ 9.62%)[8] as mentioned above. The explanation comes from the stability test.

*Stability test*. During the course of this investigation, significant light sensitivity of **P** under high intensity irradiation source or when exposed to room light for a long period of time was noted upon the monitoring of the absorption spectra. Moreover, no femtosecond absorption spectra and (ps-ns) time resolved fluorescence spectra (using a Streak camera) could be acquired as **P** decomposed within seconds or minutes under laser pulse irradiation. It is noteworthy that the measurements of photophysical parameters and electronic spectra were performed with fresh samples using very low power light source (*i.e.* $10^4$ time weaker than that shown in **Figure 11**). To test this instability, **P** in degassed solution of $CH_2Cl_2$ was subjected to an irradiation at $\lambda_{exc}$ = 623 nm with a flux power density of about 20 times

what is used in solar cell design (**Figure 10**). Quasi-total photo-conversion or decomposition of **P** occurs in 10 mins of irradiation. This experiment was carried out only using **P**, as it was noticed that **P'** showed a significantly lower thermal and photochemical stability.

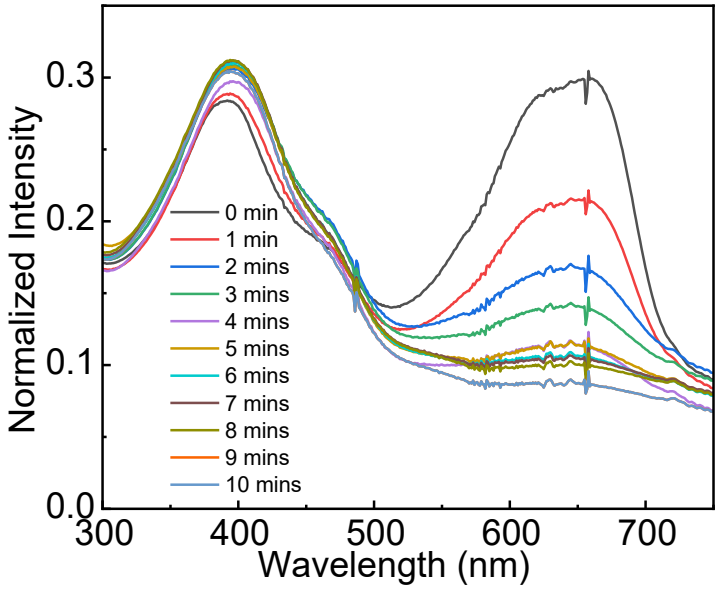


**Figure 11**. Time-dependence of the absorption spectra of **P** in $CH_2Cl_2$ upon irradiation at 623 nm (flux power density = $19.7 \times 10^3$ W/m$^2$). Note that the flux density at AM 1.5 is $1 \times 10^3$ W/m$^2$).

*Additional comment*. Recently, the PCE of **PA** (**Figure 12**) was also reported to be modest (1.64%) for a device that contained $PC_{71}BM$ as the electron acceptor.[8] The $E_{LUMO}$ and $E_{HOMO}$ are respectively -4.11 and -5.37 eV for **PA**, and -4.15 and -6.10 eV for $PC_{71}BM$. The energy gap between the two $E_{LUMO}$'s ($\Delta E_{LUMO}$) turns out to be downhill but rather small (0.04 eV). It is noteworthy that for a large downhill $\Delta E_{LUMO}$ in a reductive quenching reaction, the rate of electron transfer is faster and the PCE value is generally larger. This correlation between the small $\Delta E_{LUMO}$ and the low PCE for **P1-P5**/$PC_{61}BM$[5] *vs* **PA**/ $PC_{71}BM$[8] appears clear.

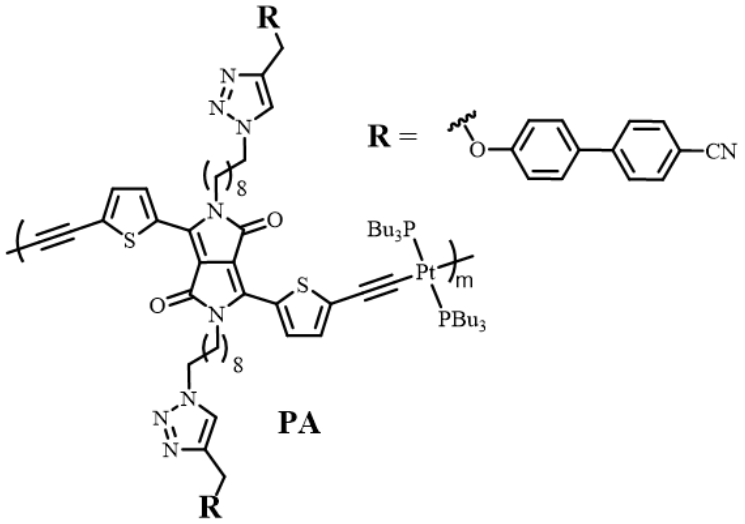


**Figure 12**, Structure of **PA**.[8]

## Conclusion

This investigation pointed at two sources seemingly responsible the low PCEs of the OSCs built with **P1-P3** previously reported by Wong and his collaborators.[5] The first one is the choice of the electron acceptor. In the former investigation, $PC_{61}BM$ was selected as electron acceptor. At that time the $E_{LUMO}$ of $PC_{61}BM$ was seemingly not considered, or at least not mentioned. It becomes clear that $PC_{71}BM$ is a better choice since its $E_{LUMO}$ is lower than that of $PC_{61}BM$. This was indeed the case for **P4** and **P5** where the PCE increased when replacing the electron acceptor $PC_{61}BM$ by $PC_{71}BM$.[6] However, this increase was mostly modest.

The second key observation is the rapid decomposition of **P**. Based on **Figure 11**, quasi-complete photodecomposition is anticipated in about 3.25 hours (197 min). Stability tests are nowadays performed in parallel with those of OSC's performance tests. The general conclusion of this investigation is that a combination of both poor selection of the electron acceptor and undetected rapid photodecomposition explain the lower PCE values of the OSC devices for **P1-P3**.

## Acknowledgement

This research was funded by the Natural Sciences and Engineering Research Council of Canada, NSERC. The authors warmly thank the french « ministère de l'enseignement supérieur, de la recherche et de l'innovation » which funded Melodie Nos and Malak

Qassab PhD as well as Normandie Université, Normandie Région, UNICAEN, ENSICAEN, CNRS, INC3M, ANR, FEDER, Normandy Region, LabEx EMC3 (ANR-10-LABX-09-01) and LabEx Synorg (ANR-11-LABX-0029) for supporting our research activities. We gratefully acknowledge K. Jarsalé for MS-ASAP-TOF. We also thank Dr. R. Herbinet for the TGA and GPC analyses and Dr. A. Vimont and Pr. A. Travert from the LCS (UMR-CNRS 6506) for UV-visible absorption measurements performed on metallooligomers thin films.

**Supporting Information**

**References**

(1) Diketopyrrolopyrrole Polymers for Organic Solar Cells Li, Weiwei; Hendriks, Koen H.; Wienk, Martijn M.; Janssen, Rene A. J. Accounts of Chemical Research (2016), 49(1), 78-85.

(2) Diketopyrrolopyrrole-based conjugated materials for non-fullerene organic solar cells Zhao, Chaowei; Guo, Yiting; Zhang, Yuefeng; Yan, Nanfu; You, Shengyong; Li, Weiwei Journal of Materials Chemistry A: Materials for Energy and Sustainability (2019), 7(17), 10174-10199.

(3) Diketopyrrolopyrrole-based functional supramolecular polymers: next-generation materials for optoelectronic applications Ghosh, Samrat; Shankar, Sreejith; Philips, Divya Susan; Ajayaghosh, Ayyappanpillai Materials Today Chemistry (2020), 16, 100242.

(4) Design of High-Mobility Diketopyrrolopyrrole-Based π-Conjugated Copolymers for Organic Thin-Film Transistors Yi, Zhengran; Wang, Shuai; Liu, Yunqi Advanced Materials (2015), 27(24), 3589-3606.

(5)Synthesis, characterization and photovoltaic properties of platinum-containing poly(aryleneethynylene) polymers with electron-deficient diketopyrrolopyrrole unit Zhan, Hongmei; Liu, Qian; So, Shu-Kong; Wong, Wai-Yeung Journal of Organometallic Chemistry (2019), 894, 1-9.

(6) Attempted inversion of semiconducting features of platinum polyyne polymers: a new approach for all-polymer solar cells Yuan, Yuping; Michinobu, Tsuyoshi; Oguma, Jun; Kato, Takehito; Miyake, Kunihito Macromolecular Chemistry and Physics (2013), 214(13), 1465-1472.

(7) A bis(diketopyrrolopyrrole) dimer-containing ligand in platinum(II) polyyne oligomers exhibiting ultrafast photoinduced electron transfer with PCBM and solar cell properties Nos, Melodie; Marineau-Plante, Gabriel; Gao, Di; Durandetti, Muriel; Hardouin, Julie; Karsenti, Paul-Ludovic; Gupta, Gaurav; Sharma, Ganesh D.; Harvey, Pierre D.; Lemouchi, Cyprien; Le Pluart, Loic Journal of Materials Chemistry C: Materials for Optical and Electronic Devices (2020), 8(7), 2363-2380.

(8) Effect of Mesogenic Side Groups on the Redox, Photophysical, and Solar Cell Properties of Diketopyrrolopyrrole-trans-bis(diphosphine)diethynylplatinum(II) Polymers Marineau-Plante, Gabriel; Nos, Melodie; Gao, Di; Durandetti, Muriel; Hardouin, Julie; Karsenti, Paul-Ludovic; Lemouchi, Cyprien; Le Pluart, Loic; Sharma, Ganesh D.; Harvey, Pierre D. ACS Applied Polymer Materials (2021), 3(2), 1087-1096.

(9) Ultrafast Photoinduced Electron Transfers in Platinum(II)-Anthraquinone Diimine Polymer/PCBM Films Juvenal, Frank; Lei, Hu; Schlachter, Adrien; Karsenti, Paul-Ludovic; Harvey, Pierre D. Journal of Physical Chemistry C (2019), 123(9), 5289-5302.

(10) Drastic effect of the substituent on the anthraquinone diimine moiety on the properties of the push-pull trans-bisphosphinebisphenylacetynylplatinum(II)-containing polymers Juvenal, Frank; Lei, Hu; Karsenti, Paul-Ludovic; Harvey, Pierre D. Journal of Organometallic Chemistry (2019), 896, 24-31.

(11) A 9.16% power conversion efficiency organic solar cell with a porphyrin conjugated polymer using a nonfullerene acceptorTanguy, Loic; Malhotra, Prateek; Singh, Surya Prakash; Brisard, Gessie; Sharma, Ganesh D.; Harvey, Pierre D. ACS Applied Materials & Interfaces (2019), 11(31), 28078-28087.

(12) Indolo- and Diindolocarbazoles in Organic Photovoltaic Cells Harvey, Pierre D.; Sharma, Ganesh D.; Witulski, Bernhard Chemistry Letters (2021), 50(7), 1345-1355.

(13) Modulation of band gap and p- versus n-semiconductor character of ADA dyes by core and acceptor group variation Nowak-Krol, Agnieszka; Wagener, Reinhard; Kraus, Felix; Mishra, Amaresh; Baeuerle, Peter; Wuerthner, Frank Organic Chemistry Frontiers (2016), 3(5), 545-555.

(14) Attempted Inversion of Semiconducting Features of Platinum Polyyne Polymers: A New Approach for All-Polymer Solar Cells Yuping Yuan; Tsuyoshi Michinobu; Jun Oguma; Takehito Kato; Kunihito Miyake Macromolecular Chemistry and Physics (2013), 214(13), 1465-1472.

(15) A bis(diketopyrrolopyrrole) dimer-containing ligand in platinum(II) polyyne oligomer exhibiting ultrafast photoinduced electron transfer with PCBM and solar cell properties Nos. Mélodie; Marineau-Plante, Gabriel; Gao, Di; Durandetti, Muriel; Karsenti, Paul-Ludovic; Gupta, Garav; Sharma, Ganesh D.; Harvey, Pierre D.; Lemouchi, Cyprien; Le Pluart, Loïc Journal of Physical Chemistry C (2020), **8**, 2363-2380.

(16) Synthesis, characterization and photovoltaic properties of platinum-containing poly(aryleneethynylene) polymers with electron-deficient diketopyrrolopyrrole unit Zhan, Hongmei; Liu, Qian; So, Shu-Kong; Wong, Wai-Yeung Journal of Organometallic Chemistry (2019), **894**, 1-9.

(17) Use of side-chain for rational design of n-type diketopyrrolopyrrole-based conjugated polymers: what did we find out? Kanimozhi, Catherine, Yaacobi-Gross, Nir; K. Burnett, Edmund; Briseno, Alejandro L.; Anthopoulos, Thomas D.; Salzner, Ulrike; Patil, Satish Physical Chemistry Chemical Physics (2014), **16** , 17253-17265.

(18) Insights into Bulk-Heterojunction Organic Solar Cells Processed from Green Solvent Du, Zhifang; Mainville, Mathieu; Vollbrecht, Joachim; Dixon, Alana L.; Schopp, Nora; Schrock, Max; Peng, Zhengxing; Huang, Jianfei; Chae, Sangmin; Ade, Harald; Leclerc, Mario; Reddy, G. N. Manjunatha; Nguyen, Thuc-Quyen Solar RRL (2021), Ahead of Print.

(19) Light-Induced Electron Paramagnetic Resonance Study of Charge Transport in Fullerene and Nonfullerene PBDB-T-Based Solar Cells Krinichnyi, Victor I.; Yudanova, Evgeniya I.;

Denisov, Nikolay N.; Konkin, Aleksei A.; Ritter, Uwe; Bogatyrenko, Victor R.; Konkin, Alexander L. Journal of Physical Chemistry C (2021), 125(22), 12224-12240.

(20) Tuning the electronic band structure of PCBM by electron irradiation Yoo, Seung Hwa; Kum, Jong Min; Cho, Sung Oh Nanoscale Research Letters (2011), 6(1), 545/1-545/7.

(21) Complementary absorbing ternary blend containing structural isomeric donor polymers for improving the performance of PC61BM-based indoor photovoltaics Chau, Hong Diem; Kwon, Na Yeon; Park, Su Hong; Hwang, Jinhyo; Kataria, Meenal; Harit, Amit Kumar; Woo, Han Young; Cho, Min Ju; Choi, Dong Hoon Polymer (2021), 221, 123606.

(22) Fullerene-non-fullerene hybrid acceptors for enhanced light absorption and electrical properties in organic solar cells Wu, Z.; Lee, S.; Jeong, S. Y.; Jee, M. H.; Lee, H. G.; Lim, C.; Wang, C.; Kim, B. J.; Woo, H. Y. Materials Today Energy (2021), 20, 100651.

(23) Charge Recycling Mechanism Through a Triplet Charge-Transfer State in Ternary-Blend Organic Solar Cells Containing a Nonfullerene AcceptorLee, Dongki; Hwang, Hyeongjin; Sin, Dong Hun; Park, Chaneui; Han, Se Gyo; Mun, Jungho; Noh, Jaebum; Kim, Sung Hyuk; Kim, Hyojung; Lee, Hansol; Lee, Chanwoo; Rho, Junsuk; Cho, Kilwon; Jeong, Mun Seok ACS Energy Letters (2021), 6(7), 2610-2618.

(24) A Ternary Organic Solar Cell with 15.6% Efficiency Containing a New DPP-based Acceptor Privado, Maria; Dahiya, Hemraj; de la Cruz, Pilar; Keshtov, Mukhamed Lostambievich; Langa, Fernando; Sharma, Ganesh D. Journal of Materials Chemistry C: Materials for Optical and Electronic Devices (2021), Ahead of Print.

(25) Ternary Polymer Solar Cells with High Open Circuit Voltage containing Fullerene and New Thieno[3',2',6,7][1]Benzothieno[3,2-b]Thieno[3,2-g][1]Benzothiophene-based Non-fullerene Small Molecule AcceptorKeshtov, Muhammed L.; Konstantinov, Igor O.; Kuklin, Sergei A.; Khokhlov, Alexsei R.; Ostapov, Ilya E.; Peregudov, Aleksander S.; Buzin, Mikhail I.; Dou, Chuandong; Dahiya, Hemraj; Sharma, Ganesh D.Energy Technology (Weinheim, Germany) (2021), 9(5), 2001100.

(26) Panchromatic Triple Organic Semiconductor Heterojunctions for Efficient Solar Cells Rodriguez-Seco, Cristina; Cabau, Lydia; Privado, Maria; de la Cruz, Pilar; Langa, Fernando; Sharma, Ganesh D.; Palomares, Emilio ACS Applied Energy Materials (2020), 3(12), 12506-12516.

(27) Manipulating electronic energy levels of wide-bandgap D-A copolymers via side-chain engineering to realize high open-circuit voltage polymer solar cells Chen, Long; Wang, Guo; Yin, Pan; Weng, Chao; Tan, Songting; Shen, Ping Synthetic Metals (2020), 265, 116413.